Journal of Contaminant Hydrology 248 (2022) 104026

Contents lists available at ScienceDirect

Journal of Contaminant Hydrology

journal homepage: www.elsevier.com/locate/jconhyd

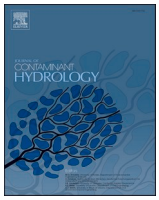

Contamination presence and dynamics at a polluted site: Spatial analysis of integrated data and joint conceptual modeling approach

Paolo Ciampi [a,h,*], Carlo Esposito [a,h], Giorgio Cassiani [b], Gian Piero Deidda [c], Adrian Flores-Orozco [d], Paolo Rizzetto [e], Andrea Chiappa [f], Manuele Bernabei [f], Andrea Gardon [f], Marco Petrangeli Papini [g,h]

[a] Department of Earth Sciences, Sapienza University of Rome, Piazzale Aldo Moro 5, 00185 Rome, Italy
[b] Department of Geosciences, University of Padua, Via Gradenigo 6, 35131 Padua, Italy
[c] Department of Civil, Environmental Engineering and Architecture, University of Cagliari, via Marengo, 2, 09123 Cagliari, Italy
[d] Department of Geodesy and Geoinformation, TU Wien, Vienna, Austria
[e] Logistic Headquarter of Italian Air Force, Viale dell'Università, 4, 00185 Rome, Italy
[f] Department of Technological Aerospace Materials–Flight Test Center of Italian Air Force, Pratica di Mare, 00071 Pomezia, Rome, Italy
[g] Department of Chemistry, Sapienza University of Rome, Piazzale Aldo Moro 5, 00185 Rome, Italy
[h] CERI Research Center, Sapienza University of Rome, Piazzale Aldo Moro 5, 00185 Rome, Italy

ARTICLE INFO

Keywords:
Hydrocarbon contamination
3D modeling
Multi-source geodatabase
Laser-induced fluorescence
Electrical resistivity tomography

ABSTRACT

Contaminated sites are complex systems posing challenges for their characterization as both contaminant distribution and hydrogeological properties vary markedly at the metric scale, yet may extend over broad areas, with serious issues of spatial under-sampling in the space. Characterization with sufficient spatial resolution is thus, one of the main concerns and still open areas of research. To this end, the joint use of direct and indirect (i.e., geophysical) investigation methods is a very promising approach. This paper presents a case study aspiring to demonstrate the benefit of a multidisciplinary approach in the characterization of a hydrocarbon-contaminated site. Detailed multi-source data, collected via stratigraphic boreholes, laser-induced fluorescence (LIF) surveys, electrical resistivity tomography (ERT) prospecting, groundwater hydrochemical monitoring, and gas chromatography–mass spectrometry (GC–MS) analyses were compiled into an interactive big-data package for modeling activities. The final product is a comprehensive conceptual hydro-geophysical model overlapping multi-modality data and capturing hydrogeological and geophysical structures, as well as contamination distribution in space and dynamics in time. The convergence of knowledge in the joint model verifies the possibility of discriminating geophysical findings based on lithological features and contamination effects, unmasking the real characteristics of the pollutant, the contamination mechanisms, and the residual phase hydrocarbon sequestration linked to the hydrogeological dynamics and adopted remediation actions. The emerging conceptual site model (CSM), emphasizing the necessity of a large amount of multi-source data for its reliable, high-resolution reconstruction, appears as the necessary tool for the design of remedial actions, as well as for the monitoring of remediation performance.

1. Introduction

Contamination and hazards related to leaking underground fuel storage tanks represent an open environmental problem that needs to be addressed through the investigation and remediation of petroleum hydrocarbon sites (Ghosh et al., 2019; Mccall et al., 2018). Petroleum hydrocarbons are part of the contaminant class known as light non-aqueous phase liquids (LNAPLs) (Vasudevan et al., 2016). These widespread and persistent pollutants are typically released into the environment as mixtures of various chemical compounds (Åslund et al., 2013). Furthermore, LNAPL aging and weathering induce mutations in the composition of the mixture, resulting in an impoverishment of both

* Corresponding author at: Department of Earth Sciences, Sapienza University of Rome, Piazzale Aldo Moro 5, 00185 Rome, Italy.
E-mail addresses: paolo.ciampi@uniroma1.it (P. Ciampi), carlo.esposito@uniroma1.it (C. Esposito), giorgio.cassiani@unipd.it (G. Cassiani), gpdeidda@unica.it (G.P. Deidda), adrian.flores-orozco@geo.tuwien.ac.at (A. Flores-Orozco), paolo.rizzetto@am.difesa.it (P. Rizzetto), andrea.chiappa@am.difesa.it (A. Chiappa), manuele.bernabei@am.difesa.it (M. Bernabei), andrea.gardon@am.difesa.it (A. Gardon), marco.petrangelipapini@uniroma1.it (M. Petrangeli Papini).

https://doi.org/10.1016/j.jconhyd.2022.104026
Received 4 September 2021; Received in revised form 6 May 2022; Accepted 7 May 2022
Available online 12 May 2022

volatile and soluble chemicals (Totsche et al., 2003), thus accumulating toxic, semi-, and non-volatile, insoluble constituents of heavier molecular weight (Lari et al., 2019). This last aspect tends to affect the selection of a reasonable characterization method and the choice of an appropriate approach for remediation (Brusseau, 2019; Suthersan et al., 2016).

An adequate characterization of the nature, chemical transformation, and spatial distribution of LNAPLs in the subsurface is one of the main open research questions (Lari et al., 2018; Totsche et al., 2003). Detailed local data may be obtained through core and borehole surveys, but such evidence is inherently 1D and unevenly distributed (e.g., Deiana et al., 2007). Field studies highlight the limitations and substantial errors that result from the use of traditional prospecting techniques (i.e., soil coring and groundwater monitoring) in estimating the amount and spatial extent of LNAPLs in the subsurface (Algreen et al., 2015). Investigations with direct methods are affected by the limited number of samples across a 3D potentially contaminated space (the subsoil) inevitably leading to spatial aliasing and inaccurate reconstruction of the pollution spatial extent (Binley et al., 2015; Cassiani et al., 2014; Ciampi et al., 2021b; Crook et al., 2008; Deiana et al., 2007; Mccall et al., 2018). Aliasing occurs when the sampling frequency is inadequately low compared with the frequency of signal variation (Shannon, 1949). As a result of spatial aliasing, the sampled variable assumes smooth variations in space, with a spatial frequency that is much lower than the true one, thus appearing different from what reality is (i.e., an alias). The impact of such aliasing on the assessment of the contamination extent and total pollutant mass is dramatic, resulting in the overestimation of contaminated volumes and pollutant masses. Correspondingly, geophysical methods capture the subsurface with high spatial resolution, permitting to depict hydrogeological heterogeneities (Ruggeri et al., 2014), and define confining geological structures which control groundwater flow and contaminant migration. Hence, geophysical methods are potentially able to bridge the gap between resolution and coverage associated with conventional hydrological investigations (e.g., Crook et al., 2008). Geophysical investigations may characterize the distribution of a plume with high LNAPL concentration (Bücker et al., 2017; Caterina et al., 2017; Flores Orozco et al., 2012, 2015, 2019a, 2019b, 2021; Xia et al., 2021), monitor LNAPL leaks and the evolution of the pollution source (Shao et al., 2019) and thus avoid the interpolation of ground truth data. In the context of environmental science, geophysical techniques have become an effective instrument to assist the study of the shallow subsurface and to control hydrological dynamics and hydrochemical processes (e.g., Binley et al., 2010, 2015). A few of the distinctive advantages of geophysical exploration tools include minimizing the requirement for direct intrusive surveys (Chambers et al., 2010) and delivering spatially continuous records of subsurface geology (Samouelian et al., 2005). Some geophysical methods may emphasize potential relationships between the meaningful measured physical parameters and the hydrological and environmental crucial aspects concerning the contaminated site characterization (Cassiani et al., 2014). Site investigation using different survey techniques (boreholes and geophysical methods) in combination with an integrated approach for data interpretation can reduce the collection of redundant information (Abbaspour et al., 2000). Also, merging linear prospection methods, which assist spatialization of data, with traditional, non-substitutable point survey techniques (Binley et al., 2015; Crook et al., 2008) can go beyond the limitations arising from their distinct implementation. On the one hand, conventional investigations are expensive, invasive, one-dimensional, and usually characterized by limited densities and irregular distributions. On the other hand, geophysical techniques cannot replace in situ sampling, do not directly record lithological or contaminant properties, and require interpretation by conventional methods to avoid potential misinterpretation of findings (Arato et al., 2014). Note that the valid hydrological understanding of geophysical data is influenced by the constitutive links (e.g., petrophysical relationships) that translate recorded geophysical parameters (e.g., electrical conductivity) into hydrological properties (e.g., water and clay content) (Binley et al., 2015).

While electrical properties may be linked to lithological structure, it is extremely challenging to link geophysical signals to contamination (Binley et al., 2015). A considerable amount of experimental research on the geophysical response of contaminants has revealed a gap in understanding a comprehensive physicochemical framework capable of relating geophysical signatures and directly measured pollutant characteristics (Arato et al., 2014; Binley et al., 2015; Cassiani et al., 2014; Flores Orozco et al., 2021; Prasanna et al., 2008). Due to the complexity and the large number of variables involved in physicochemical processes within polluted porous media, the pursuit for common and versatile models that couple geophysical records with contaminant features is not effective (Binley et al., 2015), and some degree of site-specific relationships have generally to be sought (Cassiani et al., 2014). In this respect, ancillary direct information about contaminant presence and state is essential. In this regard, the development of laser-induced fluorescence (LIF) technology helps to deliver direct knowledge on LNAPL migration and distribution with high resolution (Teramoto et al., 2019). LIF is a direct, real-time, and in-situ detection system for screening non-aqueous free-phase pollutants in the subsurface. LIFs measure a percentage fluorescence intensity relative to the standard calibration, known as the reference emitter (RE), which reflects the amount of oil in the pores (Teramoto et al., 2019). The LIF technology utilizes ultraviolet (UV) laser light provided by direct push boring instruments to excite polycyclic aromatic hydrocarbons (PAHs) molecules present in LNAPLs and simultaneously records the resulting fluorescence as a function of depth, enabling the semi-quantitative characterization of LNAPL distribution within the subsurface at least in terms of quasi-continuous 1D profiles with depth (Pepper et al., 2002). The LIF measurements coupled with cone penetrometer testing (CPT) have been extensively used for time- and cost-effective in situ detection of fuels and petroleum products and demonstrated their effectiveness in obtaining geophysical and geotechnical properties (via specific sondes placed on direct-push devices) of subsurface environments (Einarson et al., 2018; Gruiz et al., 2017; Pepper et al., 2002). Note that currently available LIF equipment is not designed to detect dissolved-phase contaminants (Fedotov et al., 2019). In the investigation and management of contaminated sites, the challenge is to integrate the information coming from different data sources to provide a consistent, realistic, and accurate conceptual model (Harris et al., 2004). Usually, multi-modality data analyze different parameters, in different configurations, with various investigation depths. Instead of handling each data set individually, a single, coherent image (model) should be generated. (Pollard et al., 2004). Coupled hydrogeophysical techniques aim to bridge this gap, but a knowledge harmonization procedure is still an open area of research (Binley et al., 2015). The synthesis of a huge volume of information and diverse sources of experience typically found at most polluted sites into a convergent, hybrid, and multi-source geodatabase may simply develop and enhance a model by collecting and incorporating new evidence or reinterpreting and validating available data (Binley et al., 2015; Zeng et al., 2022).

In this study, we suggest a stepwise refinement methodology to develop a comprehensive 3D conceptual site model including multi-source data gained from direct and indirect methods. The expected data-driven model contributes to the convergence of different types of spatial subsurface information (i.e., lithological, hydrogeological, geophysical, chemical, geotechnical), establishing a connection between the environmental variables to overcome both the spatial sampling limitations of direct methods and the interpretation of geophysical investigations. We aim at investigating the effectiveness of a single big-data package and multi-source hydrogeophysical model, capturing hydrogeological and geophysical evidence, as well as contamination dynamics over time. The application of data fusion has the goals to (i) reduce the uncertainty associated with subsurface interpretation, (ii) decipher geophysical findings based on geological, chemical, and

physical information, and (iii) provide compelling insights into LNAPL behavior in the saturated and unsaturated domains. The presented case study concerns contamination caused by jet fuel in a military airbase in Italy. From the approach investigated here, integration of heterogeneous data in nature and resolution demonstrates to provide additional information without the requirement for additional investigations, differentiating geophysical results based on lithologic characteristics and contamination effects as well as revealing the actual distribution and mechanisms of contamination, pollutant aging, and residual phase hydrocarbon sequestration related to hydrogeologic dynamics and adopted remediation measures.

2. Materials and methods

2.1. The case study: remediation history and available data

The study site is the military airport of Decimomannu (Cagliari, Italy), affected by jet fuel-JP8 spills due to a leaking in a fuel transfer line (Ciampi et al., 2021b). The spills have occurred in 2007 (40 m^3), in 2009 (5 m^3), and 2010 (5 m^3). The remediation/safety measure adopted at the site consists of pumping wells and a hydraulic barrier for groundwater extraction (Brusseau, 2019). During the characterization and remediation of the site, a suite of investigations has taken place (Table 1 of Supplementary Material), such as grain size analysis of cores, hydrogeological tests, geophysical surveys, groundwater samplings and analyses. In total, 85 stratigraphic boreholes were realized from 2007 to 2016 to deliver an overview of the geological sequence found at the site. They reach depths ranging from 10 m to 26 m below ground and cover an investigation area of about 26.5 ha. The deposit permeability was first estimated from the grain distributions reported in Flores Orozco et al. (2021). Additionally, two pumping tests and ten slug tests were performed as part of this work to provide a measurement of the aquifer permeability coefficient. For the monitoring of groundwater levels and contamination, 62 piezometers have been installed on-site. Periodic hydrochemical measurements were made on the piezometric network between 2011 and 2018, providing the necessary information to deduce the evolution of the hydrocarbon contaminant plume. Some comparative analyses, performed through gas chromatography–mass spectrometry (GC–MS) on "fresh" products (original jet fuel) and supernatant sporadically recovered in the piezometric network, enriched the collected data. Such analyses aimed at delivering the speciation of the hydrocarbon mixture components to research any evidence of aging or weathering (Vozka et al., 2019). Additionally, to gain direct information about the distribution of the NAPL, 30 points were surveyed using the LIF-ultraviolet optical screening tool (UVOST) technology in combination with CPT measurements.

2.2. The geophysical dataset

The geophysical dataset consists of several surface Electrical Resistivity Tomography (ERT) - (e.g., Binley and Kemna, 2005; Cassiani et al., 2014; Crook et al., 2008) - lines located both inside and outside of the base perimeter. The detailed map of the ERT investigations realized as part of this study is shown in Fig. 1 of the Supplementary Material. Two slightly different acquisition strategies were adopted:

- Line 15, which runs along the Southern side of the airbase, is a 330 m line with 1 m electrode spacing, composed of 7 individual ERT lines made of 72 electrodes each, with a partial superposition of neighboring lines of 24 electrodes;
- Lines 1–14 are single ERT lines made of 48 electrodes each, with electrode spacing equal to 1 m.

In both cases, a dipole-dipole skip-4 acquisition scheme was adopted (skipping 4 electrodes in each dipole means that the dipole lengths, for both current injection and voltage difference measurement are 5 m long). The full reciprocal acquisition was performed to assess measurement errors, as good practice for high-quality data surveys (e.g. Cassiani et al., 2006). A complete acquisition of all reciprocals (swapping potential with current electrodes) is essential for estimating the errors in the acquisition and permits the elimination of outliers before data inversion (Binley et al., 1995). The location of the ERT profiles (see Fig. 1 of the Supplementary Material for details) was decided based on the need to investigate geological constraints on contamination dynamics in areas hydrogeologically down gradient of spills and the hydraulic barrier. In particular, line 15 covers the entire Southern border of the base in the area of interest, while the other short lines sample with fine detail the areas where contamination, and thus biodegradation, is expected to be maximal, with a few lines also placed outside the expected contaminant plume to provide background (uncontaminated information). The ERT lines to the West cover for the most part, inside and outside the base fence, the region where clays are expected to be very shallow or emerge at the surface.

In all cases, inversion of ERT was conducted using the Profiler-R2 suite of programs provided by Lancaster University (http://www.es.lancs.ac.uk/people/amb/Freeware/R2/R2.htm) now incorporated in the ResIPy package (Blanchy et al., 2020). The inversion strategy is based on Occam's approach, thus obtaining the smoothest model compatible with the error in the data, in this case, equal to 5% reciprocal error.

2.3. The big-data package for multi-source geomodeling

This huge volume of different source data was then georeferenced and added into an interactive big-data package, which is structured as a multiple excel worksheet and relational database (Ciampi et al., 2019b). The developed multi-thematic, four-dimensional (4D) big-data package considers time as the fourth dimension and should permit the management, integration, and release of data during the knowledge acquisition phase (Ciampi et al., 2019a, 2021a), behaving as a decision support tool (DST) during the remediation period (see e.g., Huysegoms and Cappuyns, 2017). The big data package aided in the planning of investigations as it permitted to follow field findings, and in time-lapse monitoring of remediation actions at the pilot-scale described by Ciampi et al., 2021b. Grid and block spatial modeling of multidisciplinary data contained in the geodatabase has the purpose of generating a multi-source conceptual model in 2D or 3D, containing geological, hydrochemical, and geophysical information (Ciampi et al., 2021b; Wang and Huang, 2012). The 3D conceptualization of spatial and physical parameters was built using the RockWorks 17 software (Ciampi et al., 2019b). The reconstruction of a solid model that overlays different types of knowledge arises from the spatial interpolation and joint processing of the geological, geophysical, and hydrochemical parameters (Kaliraj et al., 2015; Safarbeiranvnd et al., 2018). The parameters include stratigraphic borehole data (depth and lithological types), groundwater level elevations, LIF data (percentage fluorescence intensity), geophysical information (resistivity), geotechnical records (cone resistance), and the chemical analysis of water sampled (contaminant concentration). The interpolation of all the above point data was performed using the algorithm of inverse distance weighting (Mirzaei and Sakizadeh, 2016; Safarbeiranvnd et al., 2018) to generate quasi-continuous 3D models (and 2D canvas), in which the spatial distribution of the parameters obtained from all investigations is easily accessible. The inverse squared distance (weighting exponent of 2) was used and the search neighborhood was limited to 4 points, so that the extrapolated value gradually approaches the value of the nearest sample point, honoring the data value (Liu et al., 2020). Additional options included a high fidelity filter to preserve control point values and low smoothing (Falivene et al., 2010). Joint grid and block modeling, which employs elementary volumes (voxels) in a three-dimensional mesh, aims to store, overlay, and represent multi-source information related to stratigraphic, piezometric, resistivity, fluorescence, and cone resistance data in a geo-referenced space (Høyer et al., 2015). The 3D mesh covers the area of the airbase

and extends vertically from 8.8 m below sea level to 23.4 m above sea level, representing the maximum depth of investigation and the maximum elevation of the ground surface respectively. The solid and block geological model was built by interpolating the top and base grid surfaces of each unit listed in the database to isolate the volumes of the different strata. Spatial interpolation of water table elevations and contaminant concentrations was performed to generate the piezometric surface and contamination state contour maps. Voxel modeling was used to interpolate data acquired via ERT, LIF, and CPT. A voxel stores a single numerical value for each physical parameter assigned by interpolation to explain potential spatial relationships among aggregated complex data-driven structures. The voxel grid discretization is 0.5 m × 0.5 m × 0.2 m in the x, y, z directions. The multi-source block model has a size of 780 × 1379 × 162 voxels. These dimensions were chosen to achieve a high resolution of the mapped geological structures, consistent with the acquisition resolution of ERT investigations. Signal acquisition from LIF-CPT images was averaged at the set voxel resolution to combine multi-modality data within a unique 3D mesh domain. A distance clipping filter was employed to limit the resistivity model based on a node's distance of 5 m from the ERT lines. The integrated extraction of geological-physical attributes from each voxel of the 3D mesh and their coupled analysis was intended to geostatistically discriminate lithological structures based on electrical properties. Such a joint-modeling approach has the purpose of developing a CSM that considers extension and degree of contamination, characteristics, and chemical-physical parameters that condition the mobility and the pollutant partition among aqueous, non-aqueous, solid, and gas phases. The adopted holistic approach aims to demonstrate how the joint integration of the different investigations overcomes not only the limitations related to their single applicability but also the indirect and thus uncertain nature of non-invasive investigations.

3. Results

3.1. Geological and hydrogeological settings

In the Decimomannu airbase area, the most recent deposits are related to a Plio-Quaternary depositional sequence of alluvial sediments (Bini, 2013; Reuter et al., 2017). Building on the information collected through the execution of stratigraphic surveys and as illustrated in Fig. 1, the geological structure of the subsoil is subdivided as follows:

1. Backfill (anthropogenic) materials to a depth of 1–1.5 m;
2. Recent alluvia extending to depths between 1 m and 5 m and characterized by gravels and sands with a presence of fine fraction;
3. Intermediate clays forming a horizon of sandy-gravelly clays having hazelnut color characterized by an average thickness of 1.5 m;
4. Ancient alluvia defining a layer around 3.5 m thick (on average) comprised of gravel and sand in a silty-clay matrix;
5. Base clays found in a thick level of clays and silty clays are located at depths between 10 m and 24 m;
6. Base gravels at a depth of about 24 m from the ground surface, a horizon made of gravels and sands immersed in a silty-clayey matrix.

The reconstructed three-dimensional geological model reveals both the irregularity of the stratigraphic contacts and the geometric structures that characterize the different horizons. A vertical exaggeration factor is used to mark the lithological steps. The set of all information acquired during the phases of characterization and remediation converges within the solid geo-referenced model (Fig. 1).

The recent and ancient alluvia have a highly variable thickness and are separated by intermediate clays. The alluvial sequence hosts the shallow aquifer and overlies the base clays. Based on the particle size distribution of soil samples, the hydraulic conductivity of the coarse-grained deposits ranges from 1.8×10^{-4} and 6.5×10^{-6} m/s for the recent alluvia and between 1.7×10^{-6} to 1.9×10^{-8} m/s for the ancient alluvia as reported by Flores Orozco et al. (2021). A permeability coefficient of about 4.2×10^{-9} m/s has been attributed to the intermediate clays, while for the base clays it approximates 2.7×10^{-10} m/s. Aquifer permeability obtained by slug tests varies between 9.96×10^{-4} and 2.54×10^{-6} m/s. The aquifer permeability coefficient estimated by pumping tests ranges from 1.48×10^{-3} to 3.15×10^{-4} m/s. The base and the intermediate clays have a relevant hydrogeological role as aquiclude and aquitard, respectively. The base gravels constitute the confined aquifer, while the shallow aquifer is the most sensitive to fuel spills. In undisturbed conditions, the piezometric surface stands at 4.5 m below ground level. Groundwater flows from NE to SW and is hosted in an aquifer that exhibits variable conditions from locally phreatic to partially confined elsewhere. In such a geological context, intensive extraction by pumping wells and hydraulic barrier may potentially

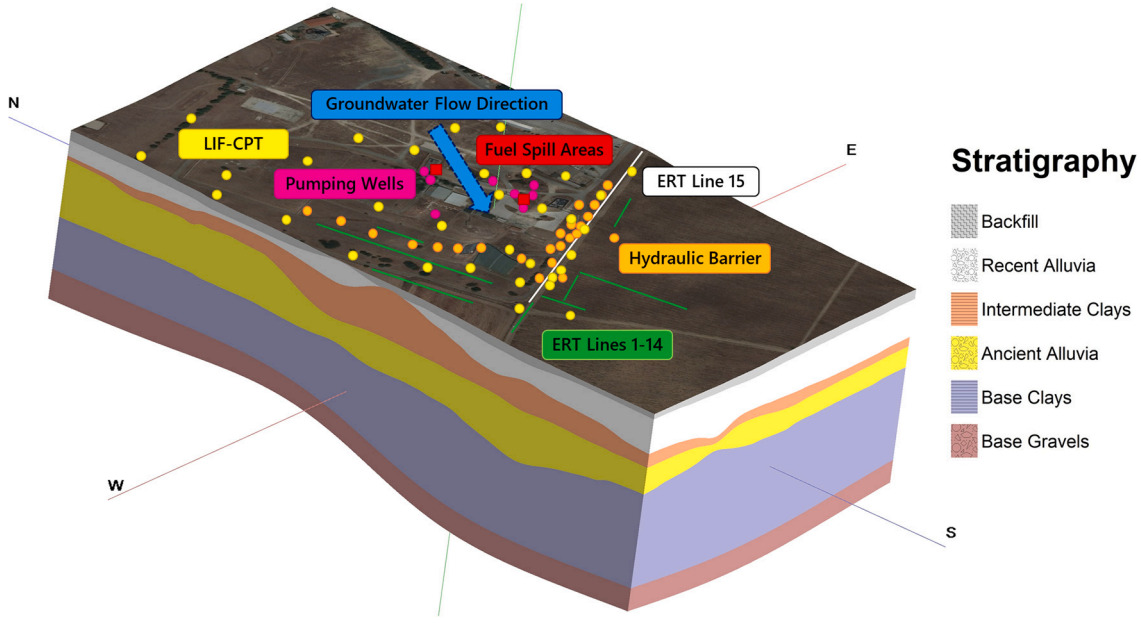

Fig. 1. Three-dimensional geological model of the Decimomannu military airbase depicting the stratigraphic relationships. Position of the fuel spill areas, pumping wells, hydraulic barrier, LIF-CPT investigations, and ERT lines inside the military domain.

trigger local modifications of groundwater head distribution and drawdowns of the water table.

3.2. Geophysical model

The acquisition and the incorporation of ERT profiles within the voxel-based and multi-source model provide the necessary data to refine and strengthen the conceptual geological model, which arises from the interpolation of point measurements. Hence, ERT data reinforces and validates stratigraphic data, and avoids potentially serious spatial aliasing effects from interpolation of borehole data above ERT resolution threshold (Binley et al., 2015; Crook et al., 2008). In particular, the overlay of voxel-based geophysical data and geological information portrays a clear correlation between the low resistivity layers and the clays. This correlation is expected due to the high surface area and surface charge of clays, which in turn contribute to surface conductivity in addition to the electrolytic conductivity (e.g., Revil et al., 2017; Flores Orozco et al., 2021). The intermediate layer of clays is of course the main structural feature affecting groundwater flow, and thus contaminant distribution, because of their very low hydraulic conductivity. The geophysical surveys concluded that the intermediate clays reach the maximum thickness in the western sector, while locally they disappear to the east, where communication of groundwaters hosted in the alluvial sediments can occur, as illustrated in Fig. 2.

The filling material reveals values of resistivity generally between 80 and 250 Ω·m (log10 resistivity range: 1.9–2.4). Coarse deposits constituting recent and ancient alluvia exhibit a variant geoelectric signature between 40 and 126 Ω·m (log10 resistivity range: 1.6–2.1). The intermediate and base clays are distinguished by an average value between ~8 and 60 Ω·m (log10 resistivity range: 0.9–1.8). The combined extraction of geological and physical properties from the mesh elements of the data-driven model provides the resistivity distribution of shallow lithologies, correlating the electrical behavior with the geological parameter (Fig. 3).

Although some lithologies reveal overlaps in resistivity signals, incorporation of ERT prospecting into the geological model discretizes geological-physical properties in space. This leads to the differentiation of geological heterogeneities with high resolution, especially in the horizontal direction, managing uncertainties arising from both sources of information. In the Western sector of the site, where the intermediate clays exhibit a larger thickness, the layers characterized by a low electrical resistivity correspond to the clayey horizons, whereas the levels with a higher electrical resistivity coincide with the sandy layers of the shallow aquifer. In the Eastern sector, the ERT profiles reveal higher electrical resistivity values (Fig. 2). In this portion of the airbase, the clayey intermediate lens is almost totally absent, with the preponderance of the recent alluvia. This affects the electrical properties of the subsoil, resulting in higher resistivity values. Therefore, even though ERT is not able to quantify the hydraulic conductivity of porous media, it aids in the discrimination between formations marked by different electrical and hydraulic resistivities (Cassiani et al., 2014). Integrating the findings of geophysical investigations into the geological model leads to the geoelectrical parametrization, the qualitative and quantitative geophysical interpretation of near-surface sediments. Accordingly, the combination of the data potentially reduces the misinterpretation of stratigraphic variations resulting from interpolation through increased density and resolution of geophysical data (Binley et al., 2015; Crook et al., 2008; Hermans and Irving, 2017). Statistical data analysis experimentally explores the results of the multi-source models, correlating the stratigraphy of mesh elements with their resistivity distribution and providing an explanation of the electrical behavior based on the knowledge of the lithological parameter.

Locally, the superposition of the geoelectric response does not allow for the discretization of deeper sediments. This effect is observed in the hydrogeologically downstream portions of the spills. However, in such areas, the geophysical model shows locally low resistivity values in the upper levels. The latter variations can be observed in Fig. 4 at a depth between 1.5 and 4 m, in correspondence with some bands with a resistivity between 16 and 40 Ω·m (log10 resistivity range: 1.2–1.6). From the cross-validation of the geological-geophysical section shown in Fig. 5, it appears plausible to hypothesize that the pronounced increase in electrical conductivity may be associated with biodegradation activity at shallow sediments impacted by petroleum hydrocarbons rather than geological heterogeneity (see Cassiani et al., 2014, and references therein).

The conceptual geological-geophysical model demonstrates qualitative and quantitative discrimination of ERT results based on lithologic characteristics and contamination effects.

3.3. Evolution of groundwater quality

Utilizing total petroleum hydrocarbons (TPH) as the revealing pollution parameter, thematic maps have been constructed using the big-data package. From 2011, the detected contamination appears to be

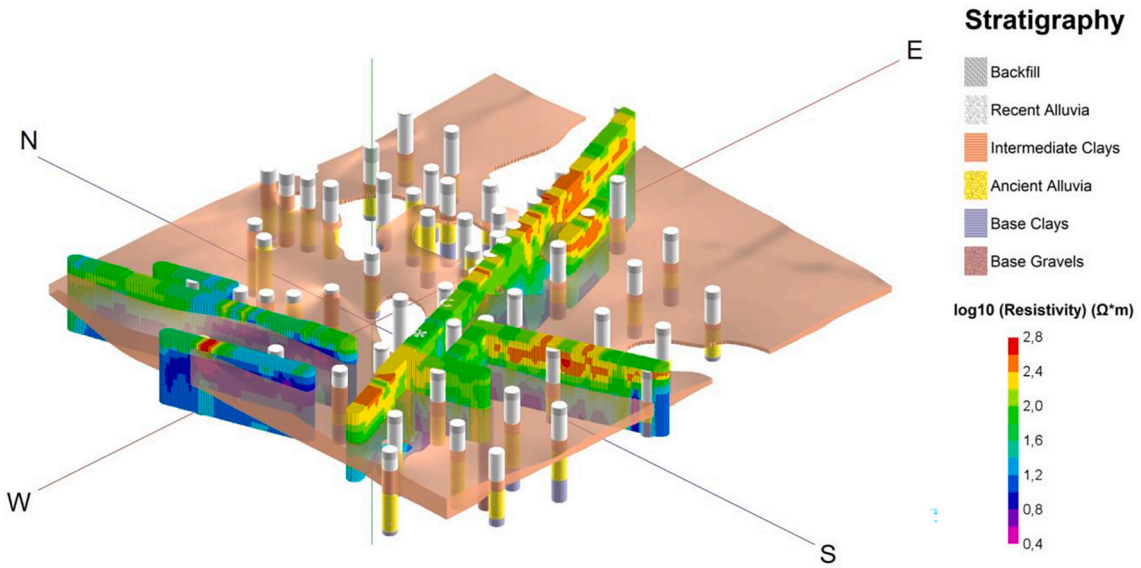

Fig. 2. Integrated three-dimensional model illustrating the results of the geophysical surveys, the layer of intermediate clays, and the stratigraphic logs.

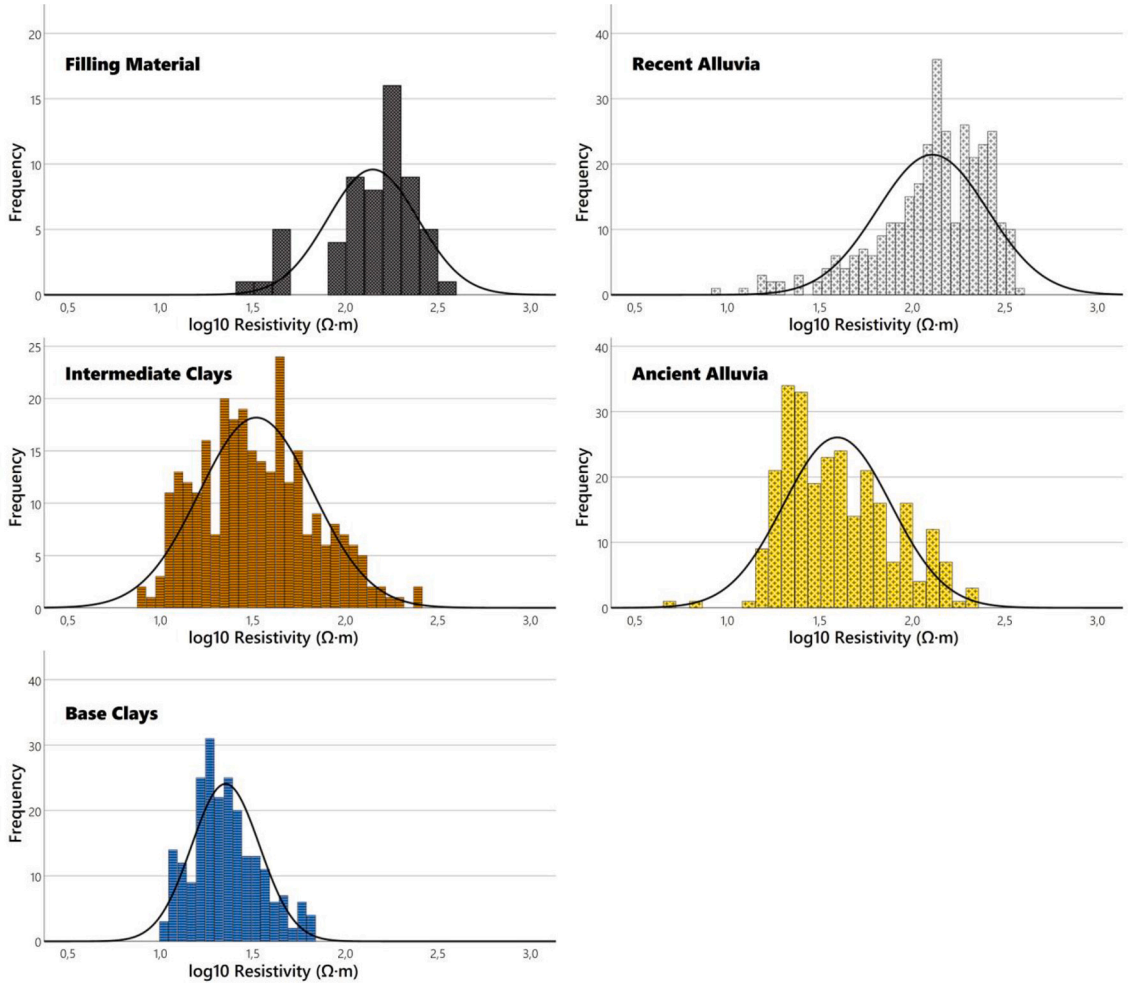

Fig. 3. Frequency histograms related to the resistivity (in log scale) of the mesh elements encoding the geological information for the different stratigraphic horizons.

fairly widespread and has been the target of years of a pump and treat action (still operational). Such remediation has allowed both a reduction of the contaminant mass and a restriction of the contaminant plume, which gradually reached an asymptotic pattern (Ciampi et al., 2021b). The thematic maps presented in Fig. 5 reveal a decrease in pollutant concentrations and the plume shrinkage over time.

The evolutionary scenario reveals a decrease in TPH concentrations from values locally approximating 1 g/L (2011) to a few mg/L (2018), hinting at the aging of the primary contamination source (Ciampi et al., 2021b). In the last represented monitoring campaign, limited areas show the impact of significant dissolved concentrations in groundwater (exceeding the limits established by Italian regulations). Such areas are mainly found at piezometers located within the tank storage area and around the hydraulic barrier zone. Here monitoring wells locally exhibit a measured concentration of TPH between 350 and 3500 μg/L. This phenomenon is likely to be linked to the production of bio-surfactants by micro-organisms rendering oily substances more bio-available (see e.g., Cassiani et al., 2014). These "critical" areas have been both historically affected by the presence of TPH in groundwater and by the infrequent appearance of LNAPL as a separate phase. Variable apparent thicknesses of supernatant (up to 1 m) were rarely detected in monitoring piezometers until 2013 (near the spill points and the hydraulic barrier). A sporadic sampling of limited apparent thicknesses (less than 1 cm) of separated phase at extraction wells has been recorded since 2014.

3.4. Analytical evidence disclosing the source-aging scenario

The multi-source big-data package was enriched by detailed speciation, through GC–MS (Vozka et al., 2019), of supernatant that has been occasionally detected in the piezometric monitoring network. The chromatograms of jet fuel and supernatant samples show a significant difference in the fingerprint regarding the peaks of more volatile fractions, less present in the supernatant, coherently with the expected aging of the contaminant separate phase (Fig. 6a, b). Besides, comparing the GC/MS chromatographic fingerprint of jet fuel and supernatant samples, a clear difference is noted for all linear components that are drastically reduced in the supernatant. This is not surprising, as these fractions are known to be more bioavailable to biodegradation (Tran et al., 2018) (Fig. 6c, d).

GC–MS analysis demonstrates that the medium-light aromatic fractions (C8- such as toluene, xylene, etc.) are nearly completely absent in the supernatant sample (Tran et al., 2018). For medium-heavy compounds (C10-es. butylbenzene, tetramethylbenzene) the phenomenon is much less pronounced (Fig. 7).

The analysis of dissolved components in water confirms the aging of the LNAPL phase. These laboratory tests were performed on a sample of water previously partitioned with supernatant and jet fuel in equilibrium conditions (Fig. 8).

The analytical investigations for water samples in contact with the supernatant and the jet fuel exhibit a very low presence of light aromatic fractions in the first case. Such an aspect reveals the exhaustion of the soluble fraction in the recovered separated phase sample. The

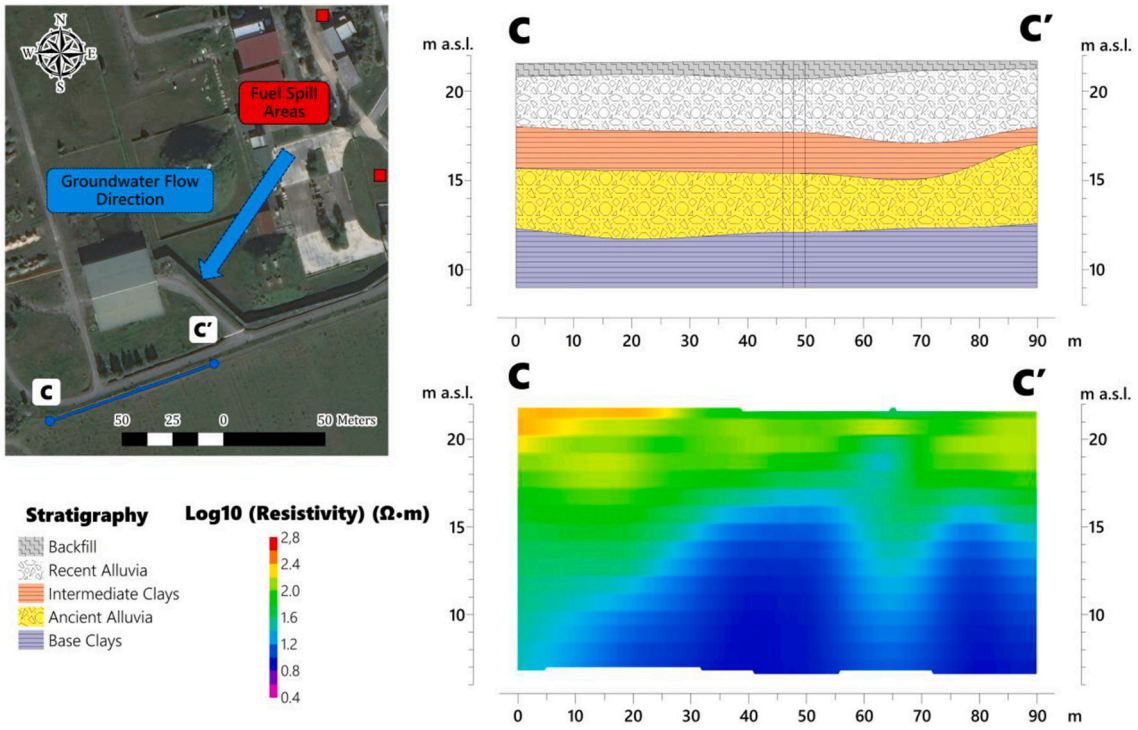

Fig. 4. Comparison of a stratigraphic and a geophysical section extrapolated from the big-data package at a trace located hydrogeologically downstream of the jet fuel spills.

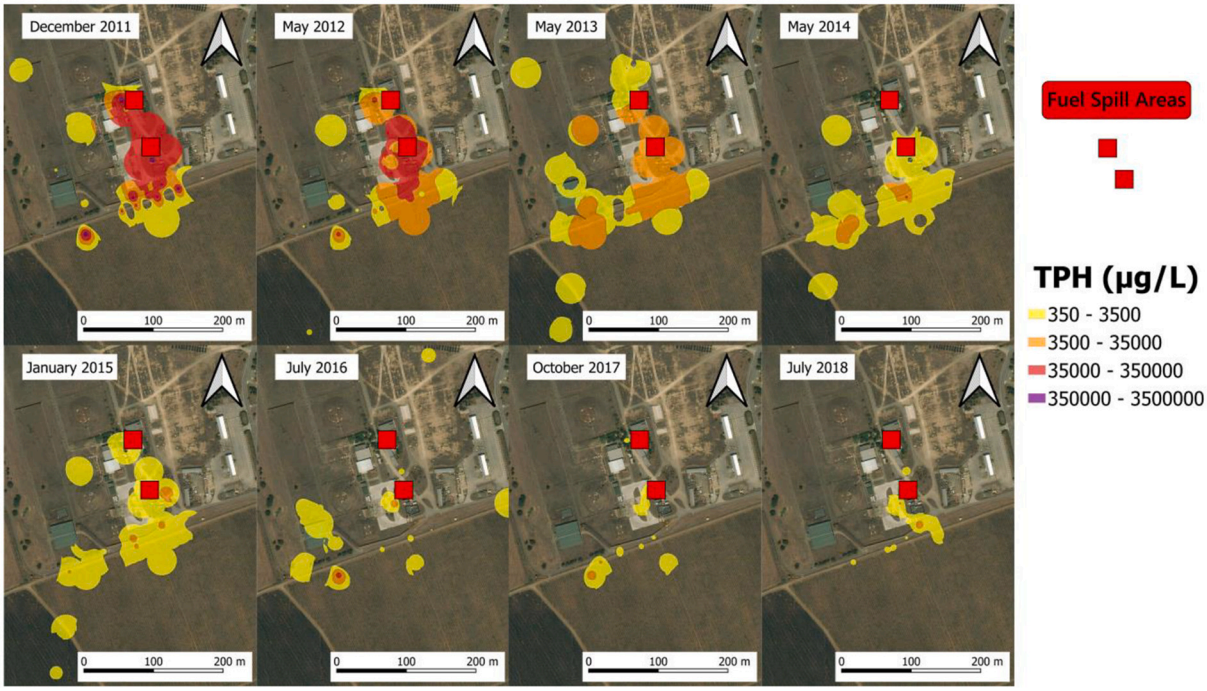

Fig. 5. Contour maps of TPH concentrations in groundwater from 2011 to 2018.

exhaustion of the more mobile and degradable components with the accumulation of the heavier fraction is associated with the natural and progressive "aging" of the contamination source (Lekmine et al., 2017). This source-aging scenario is highly representative of petroleum hydrocarbon pollution, since the composition of these mixtures, which contain compounds distinguished by widely differing chemical/physical and biodegradable characteristics, is highly complex (Vozka et al., 2019). The lighter, more soluble hydrocarbon fractions (e.g., BTEX) are mobilized into groundwater in the initial step of the primary pollution event, and aerobic biodegradation processes act on the more degradable components. The comparative analyses conducted on "fresh" product (original jet fuel) and supernatant recovered during the monitoring campaigns unmasked the presence of a weathered and aged product in the residual phase (Lekmine et al., 2017). This residual fraction, albeit

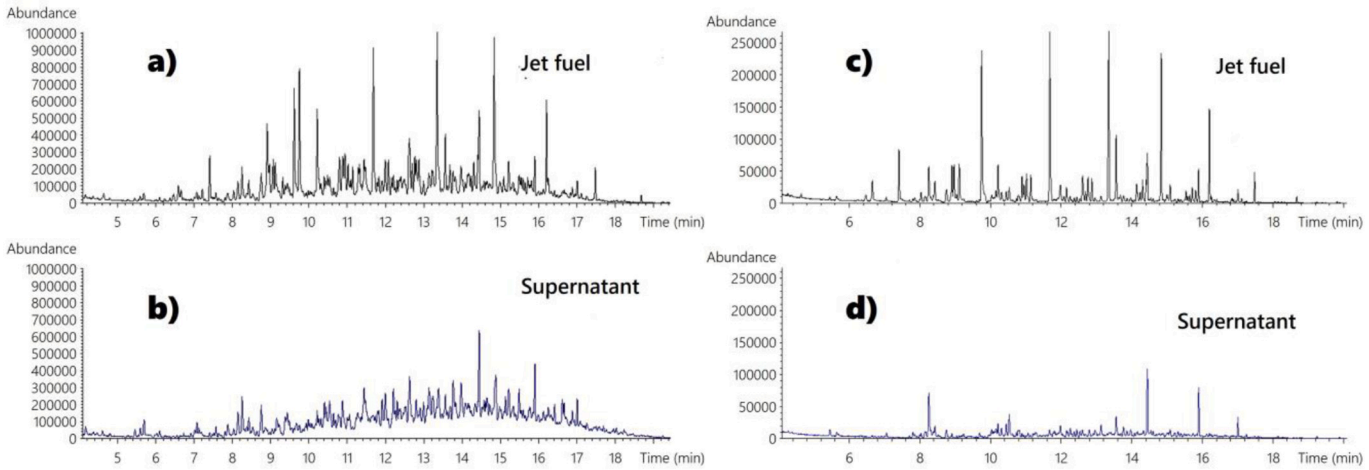

Fig. 6. GC/MS chromatographic fingerprints (total ion) related to jet fuel (a) and supernatant (b) that was occasionally collected as a free phase in the piezometric monitoring network. GC/MS chromatographic fingerprint relative to linear aliphatics (C6 – C16) measured in the "fresh" jet fuel (c) and the supernatant (d).

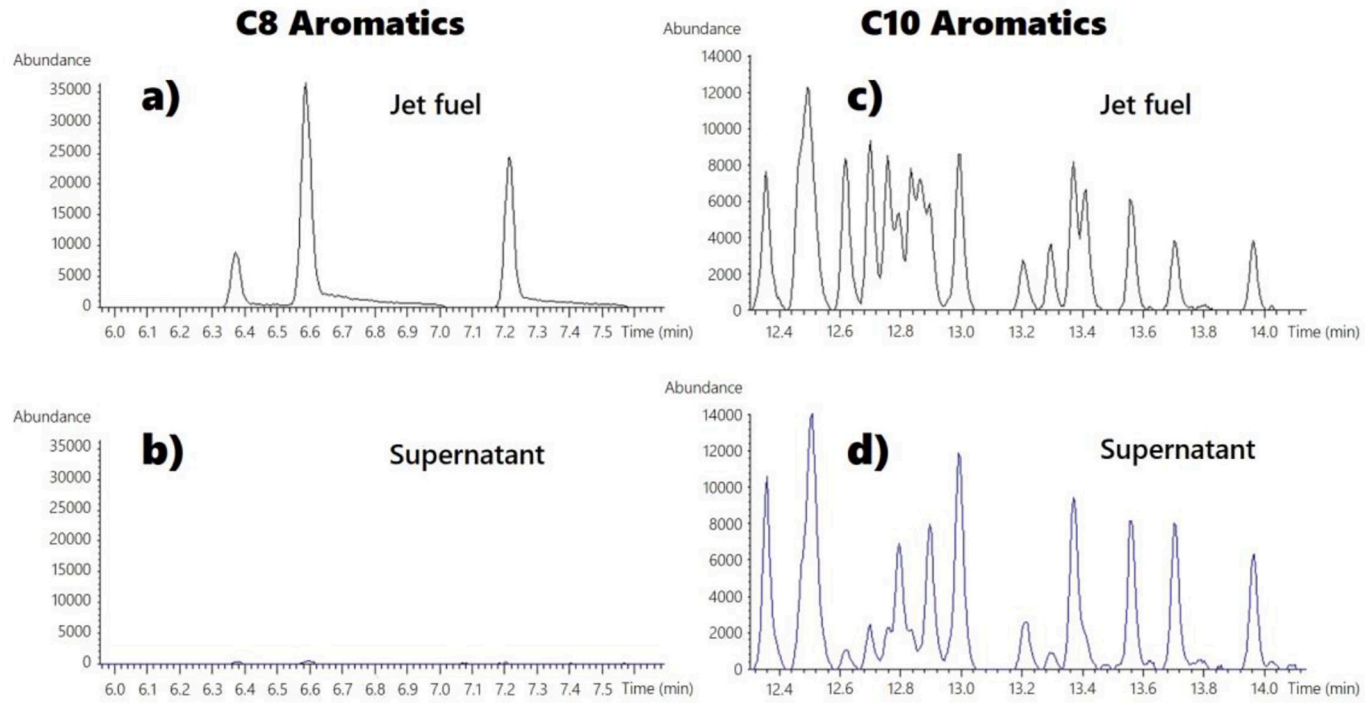

Fig. 7. GC–MS analysis of medium-light (a, c) and medium-heavy (b, d) aromatic fractions measured in the jet fuel (a, b) and the ex-situ extracted free phase (c, d).

still present in the environmental matrices, is not able to release significant quantities of soluble substances into groundwater. This latter aspect is confirmed by the total absence of the aromatic fraction in the supernatant. However, the residual, insoluble fraction of higher molecular weight hydrocarbons persists in the primary source area. This is sporadically "mobilized" and hence caught during dynamic sampling activities (Ciampi et al., 2021b).

3.5. The findings from LIF-UVOST and CPT surveys

The investigation through the LIF technique delineated the presence of the residual fraction of spilled fuel in the subsurface. Qualitative calibration of direct push profiles with spatially adjacent stratigraphic logs validates the lithotechnical interpretation (Gruiz et al., 2017). Although geologic model interpolation is not constrained by CPT data, the overlap of such data differing in nature and resolution accounts for vertical heterogeneity. The extraction of such data from the multi-source model captures lithotechnical parameterization and spatial variability of the stratigraphic profile (Einarson et al., 2018; Pepper et al., 2002) (Fig. 9).

The LIF-CPT11a presented in Fig. 9 reveals several peaks in a depth range between 6.48 m and 7.05 m, with an intensity reaching a maximum value of 25%. Some appreciable fluorescence signals, observed at depths between 10.42 m and 10.82 m with an average intensity of 4%, suggest that the spilled product may have potentially and locally reached the basement clays. Also, Fig. 9 displays an example of the CPT response as a function of depth in presence of different lithologies, depicting a major difference between coarse-grained (recent and ancient alluvia) and fine-grained (intermediate and base clays) deposits. Coarse-grained deposits exhibit cone penetration resistance values generally between 20 and 60 Mpa. Intermediate and base clays always show cone penetration resistance values below 10 MPa. The direct

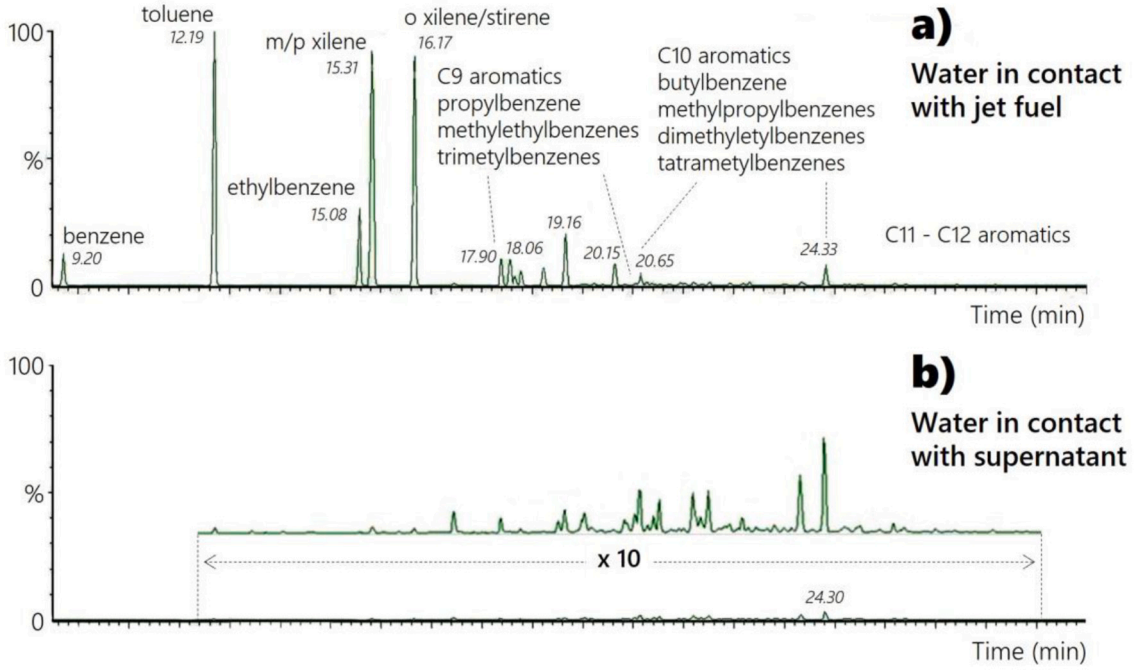

Fig. 8. Solubilization of components in water for jet fuel (a) and the supernatant (b).

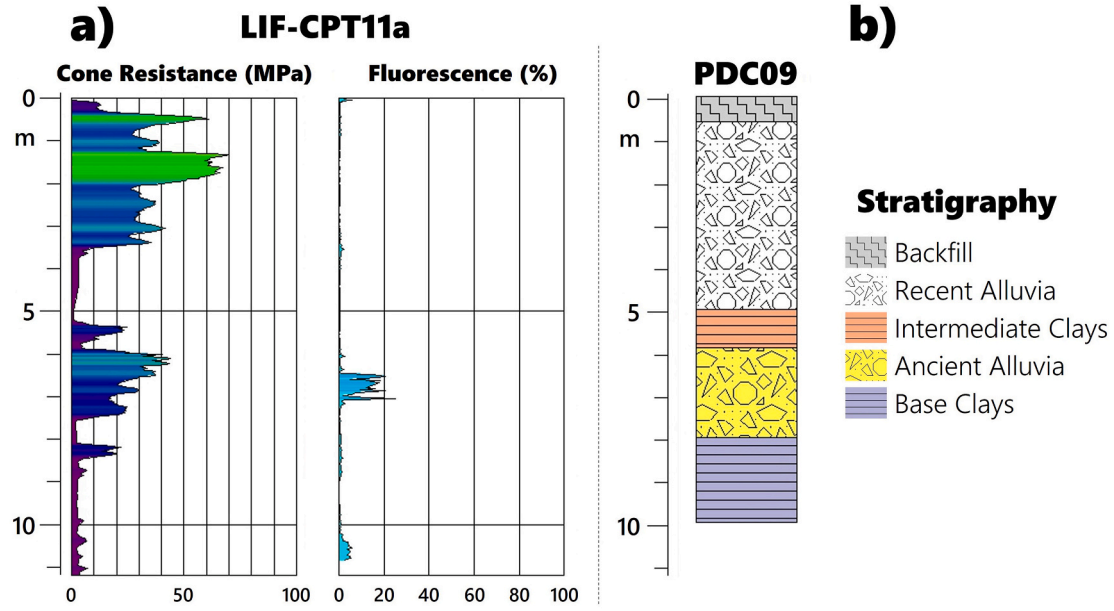

Fig. 9. Resistance to penetration of the cone resulting from CPT and fluorescence signals detected by LIF-UVOST technology along with a vertical profile (a). Adjacent stratigraphic log representing the calibration borehole (b).

geotechnical investigations validate the geological and geophysical characterization, thus, improving, in general, the integrated multidisciplinary model. The geotechnical voxel-based model exhibits an excellent correlation between the low cone resistance bands and the levels ascribable to the intermediate clays in the Western area. Differently, in the Eastern portion, cone resistance increase is due to the presence of the gravel levels belonging to the ancient and recent alluvia, as presented in Fig. 10.

The execution of 30 LIF-UVOST soundings permitted to identify with high vertical resolution the presence of contaminants as free-phase droplets or adsorbed on the solid matrix. Accordingly, the LIF investigations delineate the areas impacted by secondary and residual contamination and thus recognize the subsoil thickness affected by the presence of aged product in the geological domain (Algreen et al., 2015), as illustrated in Fig. 11.

3.6. The joint integration of multi-source data revealing the contamination dynamics

Extracting the overlapped hydrogeophysical knowledge from the big-data package yields important information about the contamination mechanisms which is not accessible without the proposed approach. In the primary source area, the free phase contaminant is present both as oil droplets trapped in the pore space and adsorbed onto the solid matrix

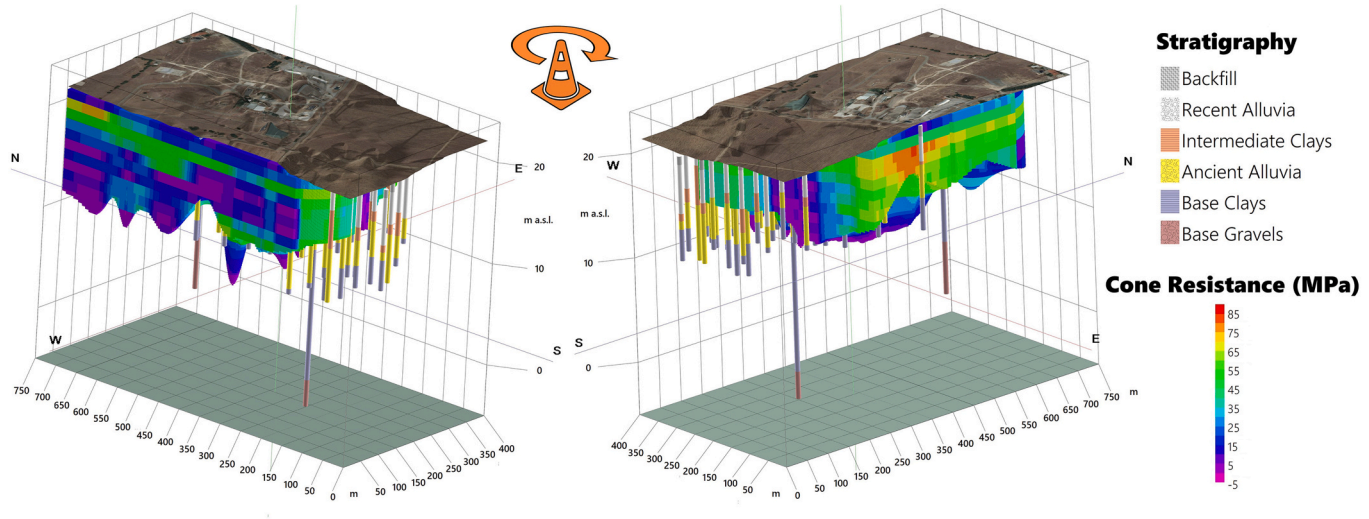

Fig. 10. Two viewpoints of the 3D geotechnical model illustrating the resistance to penetration (MPa) of the CPT cone arising from the LIF-CPT surveys and representation of the realized geological boreholes.

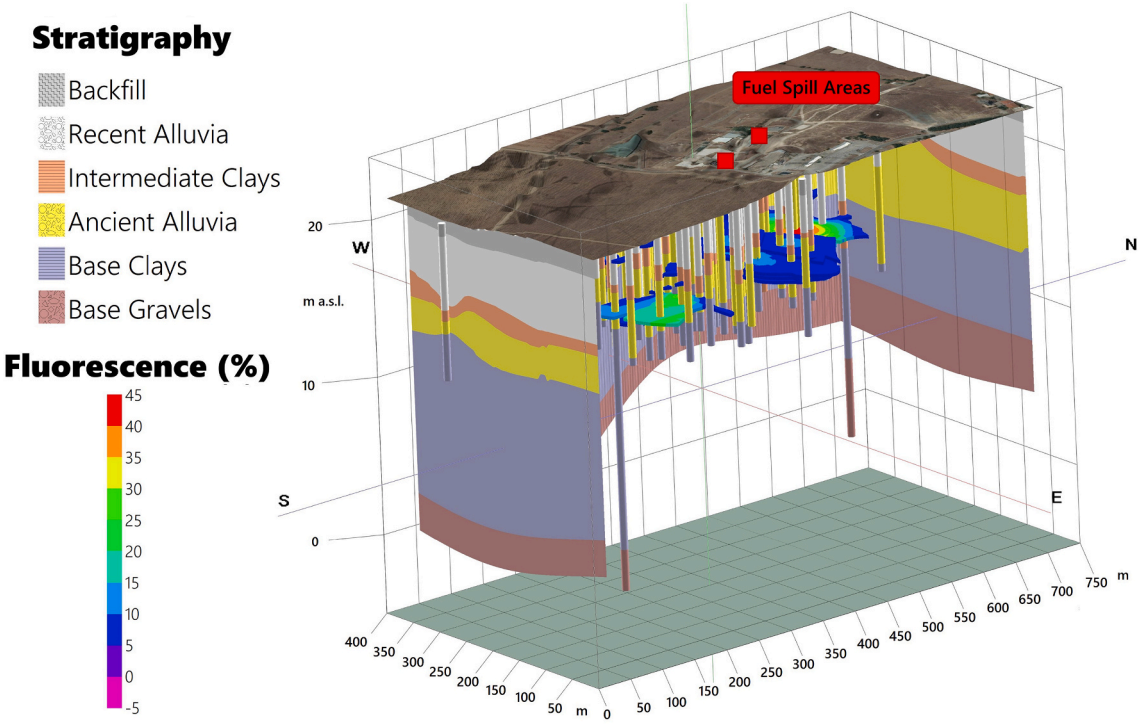

Fig. 11. 3D model of fluorescence measured by LIF-UVOST probes in the geological framework of the site. The executed stratigraphic boreholes are portrayed in the three-dimensional solid and multi-source picture.

(Trulli et al., 2016). Such contaminant is distributed across the so-called smear zone, often with a thickness of 4 m (Fig. 12).

Relatively high fluorescence signals are measured in the LIF-UVOST15 survey at depths ranging from 5.58 to 6.77 m, with a maximum peak (54% of fluorescence) at 6.02 m depth. The LIF-UVOST16 survey records moderate signals (a maximum fluorescence peak of 10%), over a depth range of 3.76 to 5.57 m. The fluorescence peaks unveil the presence of residual free-phase/adsorbed hydrocarbons in the region surrounding the water table fluctuation range, which varies between about 19 m and 14 m above sea level (Fig. 2 of Supplementary Material). Fig. 12 also reveals a potential contribution of the extraction wells on the pollution dynamics. The depression of the piezometric surface due to the pumping operated by the extraction wells and the seasonal oscillation of the water table favored the redistribution of the product in the residual phase across the smear zone (as also observed in Trulli et al., 2016) as well as laterally. The redistribution of the LNAPL along the smear zone was favored by the absence of intermediate clays in the area of the storage tanks and the pumping wells. The intercalations of intermediate clays could have limited the vertical dispersion of the contaminants caused by the changes in the water table. In the vicinity of the hydraulic barrier, the multi-source model evidences hydraulic perturbation on contamination mechanisms. The pronounced cone of depression induced by the intensive pumping favored redistribution of the aged product to the base of the aquifer and in the base clays

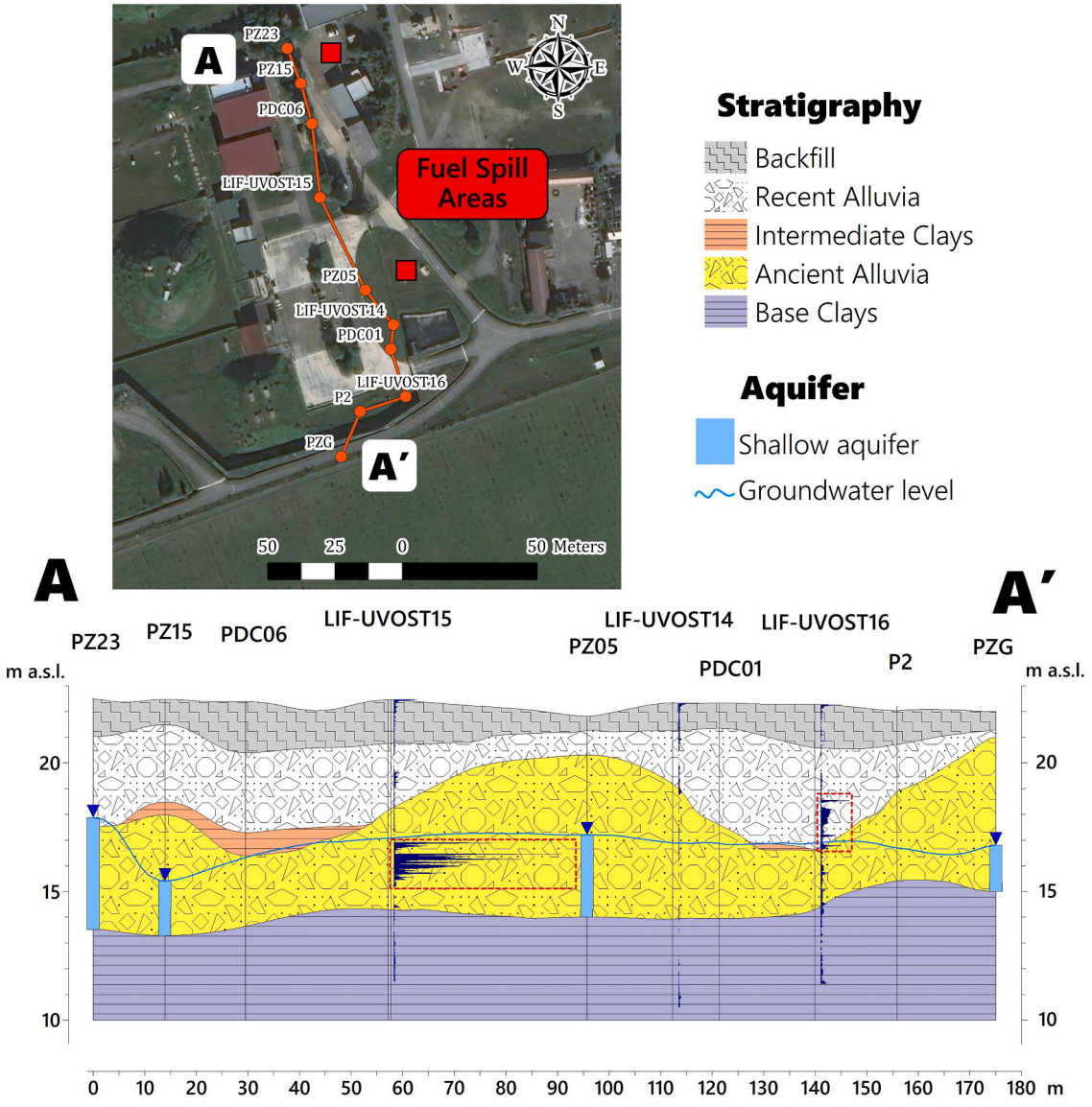

Fig. 12. Stratigraphic section, piezometric level, and fluorescence peaks detected along the track reported in the map.

(as observed in Fig. 13).

Although the presence of a peak in the low-permeability layer bounding the aquifer is unexpected, calibrating the stratigraphic profile via the ERT permits to improve the reconstruction of the aquifer conformation, by defining the geometry of the basal clay shallow interface. In such an area with a high density of input data, the geological model produced with an exact interpolator assumes the role of a training tool to develop spatial links between geological properties and geophysical signals. Although the control boreholes lie 5 m away from the ERT line and the geological model is affected by the correct interpretation of lithological data, geophysical findings reveal a substantial consistency with the geological observations at known points as well as local and abrupt deepenings of the low-permeability basal layer where interpolation failed to delineate the undulating surface of this level between stratigraphic boreholes. At borehole PB02 the resistivity section of Fig. 13 suggests a deeper contact of the base clays compared to the stratigraphic profile. Such local deviation of the geologic data from the ERT image may be related to marked lateral geologic variability over short distances or may delineate potential misinterpretations of the borehole data. The LIF detector tracks two remarkable percent fluorescence peaks at depths of 5.67 m (24%) and 7.77 m (50%). Such signals disclose the occurrence of aged product within the ancient alluvia and base clays. The overlap and interference of multiple radii of influence for intensive pumping reduced hydraulic head, dewatering the aquifer horizon. A part of the LNAPL that was originally mobile was smeared to the base of the aquifer and within the base clays due to piezometric surface depression over time (Fig. 2 of Supplementary Material). Such residual LNAPL is adsorbed to the soil particles and trapped into the pore of the saturated domain when the water table rises for aquifer recharge or recovery system pumping is reduced, providing a persistent source of groundwater contamination.

4. Discussion

The joint use of point data coming from piezometric surveys, hydrogeochemical samplings, vertical profiling of geotechnical and hydrocarbon presence (via LIF), and of spatially distributed data from ERT (i.e., geophysical) surveys led to the construction of a comprehensive 3D conceptual model concerning both (a) the hydro-geophysical structure of the site subsurface, and (b) the distribution of jet fuel contamination. This model is a tool through which the user can analyze geospatial data, giving a rapid and intuitive way to access a vast amount

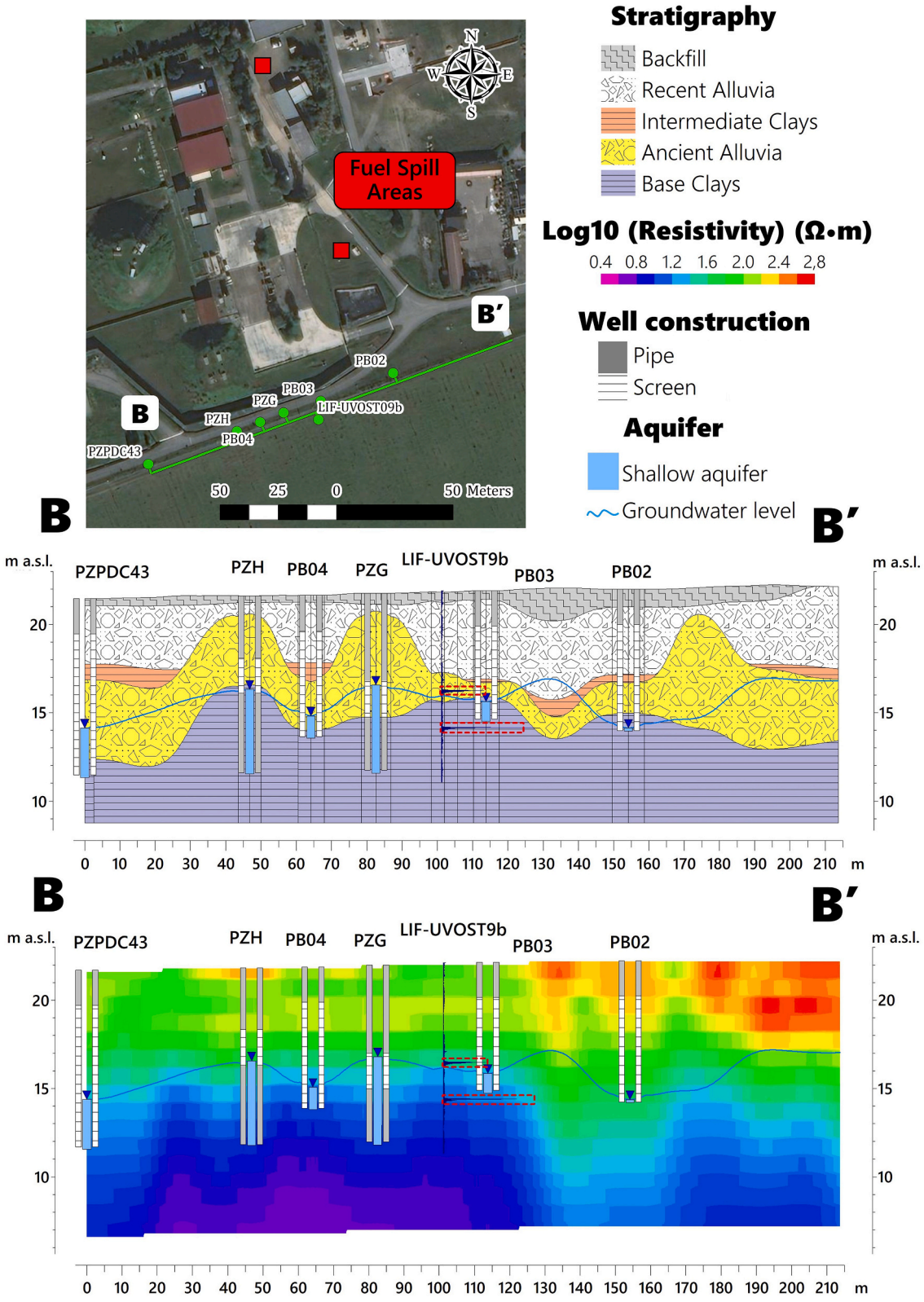

Fig. 13. Comparison between the stratigraphic and the resistivity sections which are extracted along the track reported in the map. The stratigraphy intersected by the wells, the measured piezometric level, and the recorded fluorescence peaks are overlapped on the multi-modality profiles.

of data. Such an approach has also been discussed in other studies for different areas (Ciampi et al., 2019a; Harvey et al., 2017; Jones et al., 2009). One of the main results obtained using the integrated geo-database has been to provide evidence for an improved interpretation of the ERT results based on physical information. In this regard, for our site, low electrical resistivity may be caused either by lithological features (such as clayey formations) or by contamination effects (as a result of bio attenuation) (Fig. 14).

Fig. 14 shows the cross-analysis of ERT surveys and geo-stratigraphic reconstruction from borehole cores, which allows the identification of

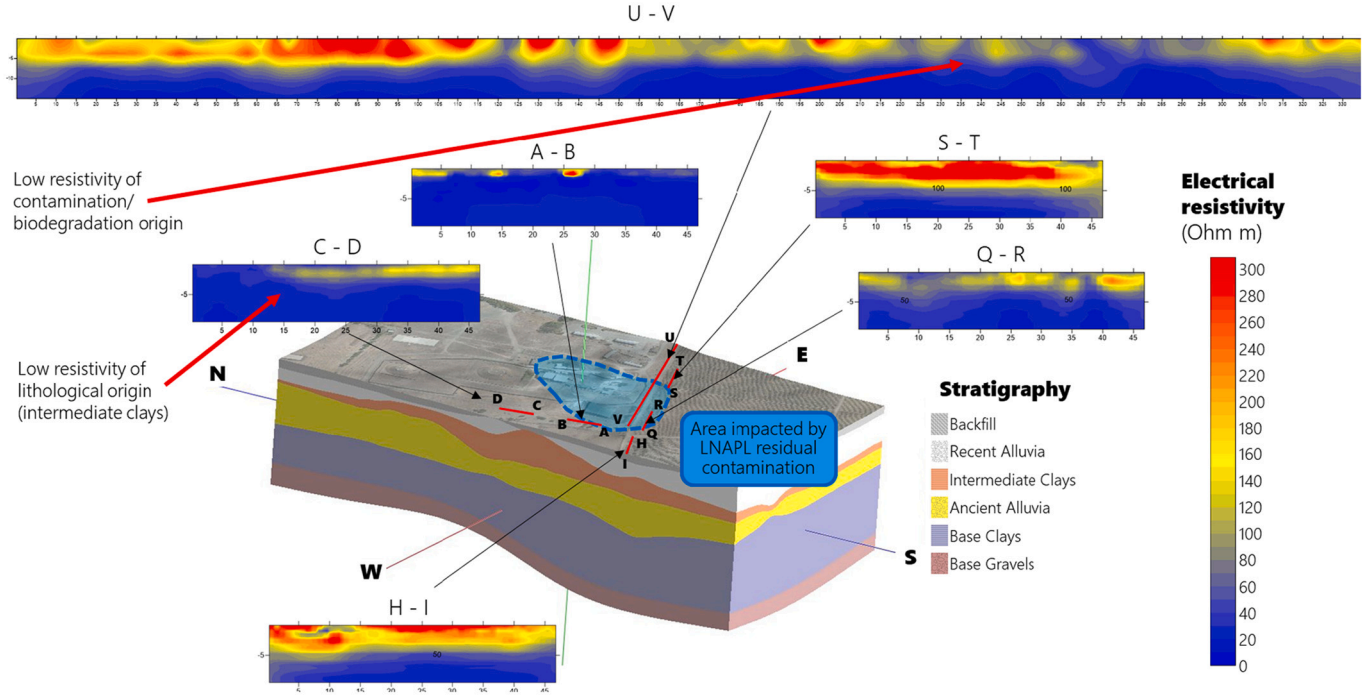

Fig. 14. Low resistivity anomalies at the Decimomannu site, caused by either (a) lithology (clays) and (b) contamination (via biodegradation).

contaminated areas. Note that without such cross-analysis the interpretation of ERT results would be impossible, in particular, to distinguish between contaminants and clays as the cause of the low electrical resistivity values. While low resistivity caused by clay is a barrier to contamination spreading, low resistivity caused by biodegradation of petroleum hydrocarbons is a viable signal of contaminant presence (e.g., Cassiani et al., 2014). The multi-source CSM provides qualitative-quantitative indicators to reduce uncertainties associated with subsurface interpretation by separating the signatures of geologic material in the absence of LNAPL (Hermans and Irving, 2017) and the substantial increase in electrical conductivity caused by petroleum hydrocarbon biodegradation (Cassiani et al., 2014). The conceptual model offers a window into in situ bioattenuation at the LNAPL-affected site and represents a tool for sharing robust evidence of microbiological activity to policymakers, who very often do not recognize natural attenuation (NA) as a remediation technology and oppose its application for limited information on natural attenuation processes (Declercq et al., 2012; Lari et al., 2019). The methods advocated in this paper could help promote a high degree of confidence and return of experience from the CSM, so NA technology could be seen as eligible by environmental authorities. Besides, the multi-source model led to the understanding of both the real pollutant characteristics and the contamination mechanisms depending on the hydraulic dynamics (Ciampi et al., 2021a). Laboratory tests proved necessary to verify the occurrence of aged product persisting in the residual phase (Lekmine et al., 2017; Vozka et al., 2019). The smearing of LNAPL caused by the water table fluctuation (Gatsios et al., 2018), the entrapment of an "immobile" phase at the base of the aquifer linked to intensive pumping, and the detection of lithotypes affected by the presence of residual product may be unveiled only by data fusion into a hydrogeophysical clone (Ciampi et al., 2021a). Again, ERTs are crucial to delineate the geometry of the base clay shallow interface, which is poorly solved by relying on borehole data exclusively. In the absence of sediment geoelectric signature spatialization, the association of a fluorescence signal to the base clays would remain approximate and uncertain. The joint-modeling findings identify the secondary contamination source that sporadically and slowly releases constituents into groundwater as a result of both piezometric surface fluctuation and horizontal groundwater flow that can cross LNAPL accumulations in the saturated aquifer (Gatsios et al., 2018; Lari et al., 2018). Such a conceptual reconstruction also explains the sporadic presence of a TPH plume downstream of the barrier, coherently with the evidence derived by Flores Orozco et al. (2021) via multi-frequency complex conductivity imaging. Future integration of complex conductivity imaging data into the multi-source model may exploit the full potential of the method adopted in this study by providing a quasi-continuous link between textural information, aquifer hydraulic properties, preferential plume transport pathways, hydrocarbon concentrations, and biogeochemical transformations via quantitative interpretation of electrical signatures of subsurface phenomena in addition to geologic contrast. Following the principles of Binley et al. (2015), Jones et al. (2009), and Crook et al. (2008), the confluence of disparate types of hydrogeophysical geomodeling develops a picture linking hydrologically relevant properties and measurable geophysical parameters of the contaminants. The fusion of multiple data sources into the data-driven model is critical to understand the underlying mechanisms that influence contamination dynamics (Ciampi et al., 2021a; Zeng et al., 2022). The fusion, exchange, and extraction of knowledge from multi-source data pursue the concepts of Breunig et al. (2020), enhancing the interoperability of multi-modal information and further advancing the utility of merged data to explain the contaminant-physicochemical behavior and guide the design of a remediation strategy tailored to site-specific characteristics. In this sense, Ciampi et al. (2021b) exploit the capabilities of the big-data package and conceptual model confined to the scale of a pilot test for 4D time-lapse monitoring of decontamination dynamics induced by reagent injection in the source area via two additional ERT profiles. Although the above study does not account for the LIF and ERT investigations reported in this work, it unveils the potential performance of the data-driven model in handling end-of-process remediation strategies, by interpreting the physicochemical modifications in space-time induced by the remediation process at the field scale and revealing the mobilization of the immobile material constituting the residual phase of hydrocarbons.

5. Conclusions

The 3D hydrogeophysical model exploits information from different

sources to discretize the different causes influencing the measured physicochemical properties, differentiating the signature of geologic features from the contamination effects and explaining pollution dynamics in space-time. GC–MS analyses unveil a source-aging scenario of petroleum hydrocarbon contamination while LIF investigations delineate the subsoil volume impacted by the presence of residual spilled fuel fraction. Incorporating electrical models from geophysical surveys into the hydrogeochemical model surmounts the limitations of spatial aliasing associated with conventional geological investigations and permits to improve the geophysical interpretation. In particular, our approach allows us to discriminate low conductivity values related to clay layers and due to aging hydrocarbon contaminants. At a contaminated site subject to remediation action through groundwater extraction wells, bridging such a gap and capturing the spatial variations of the data permits to understand the pollution mechanisms within the geological and hydraulic framework. The integrated analysis and joint data modeling approach unmask the LNAPL weathering and reveal both the trapping of residual phase hydrocarbons across the smear zone and locally to the aquifer base, due to water table fluctuation and hydraulic perturbations triggered by extraction wells. On the one hand, the redistribution and sequestration of aged contaminants in the separated phase by hydraulic processes is in agreement with the geological units and the presence of low permeability layers. On the other hand, LNAPL aging reduces the mobility of pollutants both trapped in pore spaces and adsorbed onto the solid matrix. The geodatabase-driven and multimodality portrayal emphasize the need for a large amount of multisource data to build a reliable and high-resolution conceptual model, an indispensable prerequisite for planning an effective remediation strategy.

Funding

This research did not receive any specific grant from funding agencies in the public, commercial, or not-for-profit sectors.

Data statement

Due to the sensitive nature of the questions asked in this study, the data that support the findings of this study are available from the Italian Air Force and NATO, but restrictions apply to the availability of these data, which were used under license for the current study, and so are not publicly available. Data are however available from the authors upon reasonable request and with permission of the Italian Air Force and NATO.

Declaration of Competing Interest

The authors declare that they have no known competing financial interests or personal relationships that could have appeared to influence the work reported in this paper.

Acknowledgments

We gratefully acknowledge the Italian Air Force for their support and collaboration during the data acquisition investigation and stages. We also thank the reviewers for their comments that helped to improve the quality of this manuscript.

Appendix A. Supplementary data

Supplementary data to this article can be found online at https://doi.org/10.1016/j.jconhyd.2022.104026.

References

Abbaspour, K., Matta, V., Huggenbergen, P., Johnson, C.A., 2000. A contaminated site investigation: comparison of information gained from geophysical measurements and hydrogeological modeling. J. Contam. Hydrol. 40, 365–380. https://doi.org/10.1016/S0169-7722(99)00055-8.

Algreen, M., Kalisz, M., Stalder, M., Martac, E., Krupanek, J., Trapp, S., Bartke, S., 2015. Using pre-screening methods for an effective and reliable site characterization at megasites. Environ. Sci. Pollut. Res. 22, 14673–14686. https://doi.org/10.1007/s11356-015-4649-6.

Arato, A., Wehrer, M., Biró, B., Godio, A., 2014. Integration of geophysical, geochemical and microbiological data for a comprehensive small-scale characterization of an aged LNAPL-contaminated site. Environ. Sci. Pollut. Res. 21, 8948–8963. https://doi.org/10.1007/s11356-013-2171-2.

Åslund, M.W., Stephenson, G.L., Simpson, A.J., Simpson, M.J., 2013. Comparison of earthworm responses to petroleum hydrocarbon exposure in aged field contaminated soil using traditional ecotoxicity endpoints and 1H NMR-based metabolomics. Environ. Pollut. 182, 263–268. https://doi.org/10.1016/j.envpol.2013.07.026.

Bini, C., 2013. Geology and geomorphology. In: Costantini, E., Dazzi, C. (Eds.), The Soils of Italy. World Soils Book Series. Springer, Dordrecht, pp. 39–56. https://doi.org/10.1007/978-94-007-5642-7_3.

Binley, A., Kemna, A., 2005. DC resistivity and induced polarization methods. In: Rubin, Y., Hubbard, S.S. (Eds.), Hydrogeophysics. Water Science and Technology Library, vol. 50. Springer, Dordrecht, pp. 129–156. https://doi.org/10.1007/1-4020-3102-5_5.

Binley, A., Ramirez, A., Daily, W., 1995. Regularised image reconstruction of noisy electrical resistance tomography data. In: Beck, M.S., Hoyle, B.S., Morris, M.A., Waterfall, R.C., Williams, R.A. (Eds.), Process Tomography, pp. 401–410. Proceedings of the 4th Workshop of the European Concerted Action on Process Tomography, Bergen, 6–8 April 1995.

Binley, A., Cassiani, G., Deiana, R., 2010. Hydrogeophysics: opportunities and challenges. Boll. Geofis. Teor. Appl. 51, 267–284.

Binley, A., Hubbard, S.S., Huisman, J.A., Revil, A., Robinson, D.A., Singha, K., Slater, L.D., 2015. The emergence of hydrogeophysics for improved understanding of subsurface processes over multiple scales. Water Resour. Res. 51, 3837–3866. https://doi.org/10.1002/2015WR017016.

Blanchy, G., Saneiyan, S., Boyd, J., McLachlan, P., Binley, A., 2020. ResIPy, an intuitive open source software for complex geoelectrical inversion/modeling. Comput. Geosci. 137, 104423 https://doi.org/10.1016/j.cageo.2020.104423.

Breunig, M., Bradley, P.E., Jahn, M., Kuper, P., Mazroob, N., Rösch, N., Al-Doori, M., Stefanakis, E., Jadidi, M., 2020. Geospatial data management research: progress and future directions. ISPRS Int. J. Geo-Inf. 9 (2), 95. https://doi.org/10.3390/ijgi9020095.

Brusseau, M.L., 2019. Soil and groundwater remediation. In: Brusseau, M.L., Pepper, I.L., Gerba, C.P. (Eds.), Environmental and Pollution Science. Academic Press, New York, pp. 329–335. https://doi.org/10.1016/B978-0-12-814719-1.00019-7.

Bücker, M., Flores Orozco, A., Hördt, A., Kemna, A., 2017. An analytical membrane-polarization model to predict the complex conductivity signature of immiscible liquid hydrocarbon contaminants. Near Surf. Geophys. 15 (6), 547–562. https://doi.org/10.3997/1873-0604.2017051.

Cassiani, G., Bruno, V., Villa, A., Fusi, N., Binley, A.M., 2006. A saline tracer test monitored via time-lapse surface electrical resistivity tomography. J. Appl. Geophys. 59, 244–259. https://doi.org/10.1016/j.jappgeo.2005.10.007.

Cassiani, G., Binley, A., Kemna, A., Wehrer, M., Flores Orozco, A., Deiana, R., Boaga, J., Rossi, M., Dietrich, P., Werban, U., Zschornack, L., Godio, A., Jafargandomi, A., Deidda, G.P., 2014. Noninvasive characterization of the Trecate (Italy) crude-oil contaminated site: links between contamination and geophysical signals. Environ. Sci. Pollut. Res. 21, 8914–8931. https://doi.org/10.1007/s11356-014-2494-7.

Caterina, D., Flores Orozco, A., Nguyen, F., 2017. Long-term ERT monitoring of biogeochemical changes of an aged hydrocarbon contamination. J. Contam. Hydrol. 201, 19–29. https://doi.org/10.1016/j.jconhyd.2017.04.003.

Chambers, J.E., Wilkinson, P.B., Wealthall, G.P., Loke, M.H., Dearden, R., Wilson, R., Allen, D., Ogilvy, R.D., 2010. Hydrogeophysical imaging of deposit heterogeneity and groundwater chemistry changes during DNAPL source zone bioremediation. J. Contam. Hydrol. 118 https://doi.org/10.1016/j.jconhyd.2010.07.001.

Ciampi, P., Esposito, C., Petrangeli Papini, M., 2019a. Hydrogeochemical model supporting the remediation strategy of a highly contaminated industrial site. Water 11, 1371. https://doi.org/10.3390/w11071371.

Ciampi, P., Esposito, C., Viotti, P., Boaga, J., Cassiani, G., Petrangeli Papini, M., 2019b. An integrated approach supporting remediation of an aquifer contaminated with chlorinated solvents by a combination of adsorption and biodegradation. Appl. Sci. 9 (20), 4318. https://doi.org/10.3390/app9204318.

Ciampi, P., Esposito, C., Bartsch, E., Alesi, E.J., Petrangeli Papini, M., 2021a. 3D dynamic model empowering the knowledge of the decontamination mechanisms and controlling the complex remediation strategy of a contaminated industrial site. Sci. Total Environ. 793, 148649 https://doi.org/10.1016/j.scitotenv.2021.148649.

Ciampi, P., Esposito, C., Cassiani, G., Deidda, G.P., Rizzetto, P., Petrangeli Papini, M., 2021b. A field-scale remediation of residual light non-aqueous phase liquid (LNAPL): chemical enhancers for pump and treat. Environ. Sci. Pollut. Res. 28, 35286–35296. https://doi.org/10.1007/s11356-021-14558-2.

Crook, N., Binley, A., Knight, R., Robinson, D.A., Zarnetske, J., Haggerty, R., 2008. Electrical resistivity imaging of the architecture of substream sediments. Water Resour. Res. 44 https://doi.org/10.1029/2008WR006968. W00D13.

Declercq, I., Cappuyns, V., Duclos, Y., 2012. Monitored natural attenuation (MNA) of contaminated soils: state of the art in Europe-a critical evaluation. Sci. Total Environ. 426, 393–405. https://doi.org/10.1016/j.scitotenv.2012.03.040.

Deiana, R., Cassiani, G., Kemna, A., Villa, A., Bruno, V., Bagliani, A., 2007. An experiment of non-invasive characterization of the vadose zone via water injection and cross-hole time-lapse geophysical monitoring. Near. Surf. Geophys. 5 (3), 183–194.

Einarson, M., Fure, A., Germain, R., Chapman, S., Parker, B., 2018. DyeLIFTM: a new direct-push laser-induced fluorescence sensor system for chlorinated solvent DNAPL and other non-naturally fluorescing NAPLs. Ground Water Monit. Remediat. 38, 28–42. https://doi.org/10.1111/gwmr.12296.

Falivene, O., Cabrera, L., Tolosana-Delgado, R., Alberto, S., 2010. Interpolation algorithm ranking using cross-validation and the role of smoothing effect. A coal zone example. Comput. Geosci. 36 (4), 512–519. https://doi.org/10.1016/j.cageo.2009.09.015.

Fedotov, Y., Belov, M., Kravtsov, D., Gorodnichev, V., 2019. Laser fluorescence method for detecting oil pipeline leaks at a wavelength of 355 nm. J. Opt. Technol. 86, 81–85. https://doi.org/10.1364/JOT.86.000081.

Flores Orozco, A., Kemna, A., Oberdörster, C., Zschornack, L., Leven, C., Dietrich, P., Weiss, H., 2012. Delineation of subsurface hydrocarbon contamination at a former hydrogenation plant using spectral induced polarization imaging. J. Contam. Hydrol. 136-137, 131–144. https://doi.org/10.1016/j.jconhyd.2012.06.001.

Flores Orozco, A., Velimirovic, M., Tosco, T., Kemna, A., Sapion, H., Klaas, N., Sethi, R., Leen, B., 2015. Monitoring the injection of microscale zero-valent iron particles for groundwater remediation by means of complex electrical conductivity imaging. Environ. Sci. Technol. 49, 5593–5600. https://doi.org/10.1021/acs.est.5b00208.

Flores Orozco, A., Kemna, A., Binley, A., Cassiani, G., 2019a. Analysis of time-lapse data error in complex conductivity imaging to alleviate anthropogenic noise for site characterization. Geophysics 84 (2), B181–B193. https://doi.org/10.1190/geo2017-0755.1.

Flores Orozco, A., Micić, V., Bücker, M., Gallistl, J., Hofmann, T., Nguyen, F., 2019b. Complex-conductivity monitoring to delineate aquifer pore clogging during nanoparticles injection. Geophys. J. Int. 218 (3), 1838–1852. https://doi.org/10.1093/gji/ggz255.

Flores Orozco, A., Ciampi, P., Katona, T., Censini, M., Petrangeli Papini, M., Deidda, G.P., Cassiani, G., 2021. Delineation of hydrocarbon contaminants with multi-frequency complex conductivity imaging. Sci. Total Environ. 768, 144997 https://doi.org/10.1016/j.scitotenv.2021.144997.

Gatsios, E., García-Rincón, J., Rayner, J.L., Mclaughlan, R.G., Davis, G.B., 2018. LNAPL transmissivity as a remediation metric in complex sites under water table fluctuations. J. Environ. Manag. 215, 40–48. https://doi.org/10.1016/j.jenvman.2018.03.026.

Ghosh, J., Tick, G.R., Akyol, N.H., Zhang, Y., 2019. A pore-scale investigation of heavy crude oil trapping and removal during surfactant-enhanced remediation. J. Contam. Hydrol. 223, 103471 https://doi.org/10.1016/j.jconhyd.2019.03.003.

Gruiz, K., Fenyvesi, E., Molnár, M., Feigl, V., Vaszita, E., Tolner, M., 2017. In-situ and real-time measurements for effective soil and contaminated site management. In: Gruiz, K., Meggyes, T., Fenyvesi, E. (Eds.), Engineering Tools for Environmental Risk Management. Site Assessment and Monitoring Tools. Taylor, Francis Group, CRC Press, London, pp. 245–341. https://doi.org/10.1201/b19954.

Harris, M.K., Looney, B.B., Jackson, D.G., 2004. Geology and environmental remediation: Savannah River site, South Carolina. Environ. Geosci. 11, 191–204. https://doi.org/10.1306/eg.06150404015.

Harvey, A.S., Fotopoulos, G., Hall, B., Amolins, K., 2017. Augmenting comprehension of geological relationships by integrating 3D laser scanned hand samples within a GIS environment. Comput. Geosci. 103, 152–163. https://doi.org/10.1016/j.cageo.2017.02.008.

Hermans, T., Irving, J., 2017. Facies discrimination with electrical resistivity tomography using a probabilistic methodology: effect of sensitivity and regularization. Near Surf. Geophys. 15, 13–25. https://doi.org/10.3997/1873-0604.2016047.

Høyer, A.S., Jørgensen, F., Sandersen, P.B.E., Viezzoli, A., Møller, I., 2015. 3D geological modelling of a complex buried-valley network delineated from borehole and AEM data. J. Appl. Geophys. 122, 94–102. https://doi.org/10.1016/j.jappgeo.2015.09.004.

Huysegoms, L., Cappuyns, V., 2017. Critical review of decision support tools for sustainability assessment of site remediation options. J. Environ. Manag. 196, 278–296. https://doi.org/10.1016/j.jenvman.2017.03.002.

Jones, R.R., Mccaffrey, K.J.W., Clegg, P., Wilson, R.W., Holliman, N.S., Holdsworth, R.E., Imber, J., Waggott, S., 2009. Integration of regional to outcrop digital data: 3D visualisation of multi-scale geological models. Comput. Geosci. 35, 4–18. https://doi.org/10.1016/j.cageo.2007.09.007.

Kaliraj, S., Chandrasekar, N., Peter, T.S., Selvakumar, S., Magesh, N.S., 2015. Mapping of coastal aquifer vulnerable zone in the south west coast of Kanyakumari, South India, using GIS-based DRASTIC model. Environ. Monit. Assess. 187, 4073. https://doi.org/10.1007/s10661-014-4073-2.

Lari, K.S., Rayner, J.L., Davis, G.B., 2018. Towards characterizing LNAPL remediation endpoints. J. Environ. Manag. 224, 97–105. https://doi.org/10.1016/j.jenvman.2018.07.041.

Lari, K.S., Davis, G.B., Rayner, J.L., Bastow, T.P., Puzon, G.J., 2019. Natural source zone depletion of LNAPL: a critical review supporting modelling approaches. Water Res. 157, 630–646. https://doi.org/10.1016/j.watres.2019.04.001.

Lekmine, G., Lari, K.S., Johnston, C.D., Bastow, T.P., Rayner, J.L., Davis, G.B., 2017. Evaluating the reliability of equilibrium dissolution assumption from residual gasoline in contact with water saturated sands. J. Contam. Hydrol. 196, 30–42. https://doi.org/10.1016/j.jconhyd.2016.12.003.

Liu, H., Chen, S., Hou, M., Liang, H., 2020. Improved inverse distance weighting method application considering spatial autocorrelation in 3D geological modeling. Earth Sci. Inf. 13, 619–632. https://doi.org/10.1007/s12145-019-00436-6.

Mccall, W., Christy, T.M., Pipp, D.A., Jaster, B., White, J., Goodrich, J., Fontana, J., Doxtader, S., 2018. Evaluation and application of the optical image profler (OIP) a direct push probe for photo-logging UV-induced fuorescence of petroleum hydrocarbons. Environ. Earth Sci. 77, 374. https://doi.org/10.1007/s12665-018-7442-2.

Mirzaei, R., Sakizadeh, M., 2016. Comparison of interpolation methods for the estimation of groundwater contamination in Andimeshk-shush plain, southwest of Iran. Environ. Sci. Pollut. Res. 23, 2758–2769. https://doi.org/10.1007/s11356-015-5507-.

Pepper, J.W., Wright, A.O., Kenny, J.E., 2002. In situ measurements of subsurface contaminants with a multi-channel laser-induced fluorescence system. Spectrochim. Acta A 58, 317–331. https://doi.org/10.1016/S1386-1425(01)00557-1.

Pollard, S.J.T., Brookes, A., Earl, N., Lowe, J., Kearney, T., Nathanail, C.P., 2004. Integrating decision tools for the sustainable management of land contamination. Sci. Total Environ. 325, 15–28. https://doi.org/10.1016/j.scitotenv.2003.11.017.

Prasanna, M.V., Chidambaram, S., Pethaperumal, S., Srinivasamoorthy, K., Peter, A.J., Anandhan, P., Vasanthavigar, M., 2008. Integrated geophysical and chemical study in the lower subbasin of Gadilam River, Tamilnadu, India. Environ. Geosci. 15, 145–152. https://doi.org/10.1306/eg.11080707015.

Reuter, M., Auer, G., Brandano, M., Harzhauser, M., Corda, L., Piller, W.E., 2017. Post-rift sequence architecture and stratigraphy in the Oligo–Miocene Sardinia Rift (Western Mediterranean Sea). Mar. Pet. Geol. 79, 44–63. https://doi.org/10.1016/j.marpetgeo.2016.10.025.

Revil, A., Coperey, A., Shao, Z., Florsch, N., Fabricius, I.L., Deng, Y., Delsman, J.R., Pauw, P.S., Karaoulis, M., de Louw, P.G.B., van Baaren, E.S., Dabekaussen, W., Menkovic, A., Gunnink, J.L., 2017. Complex conductivity of soils. Water Resour. Res. 53 (8), 7121–7147. https://doi.org/10.1002/2017WR020655.

Ruggeri, P., Gloaguen, E., Lefebvre, R., Irving, J., Holliger, K., 2014. Integration of hydrological and geophysical data beyond the local scale: application of Bayesian sequential simulation to field data from the Saint-Lambert-de-Lauzon site, Québec, Canada. J. Hydrol. 514, 271–280.

Safarbeiranvnd, M., Amanipoor, H., Battaleb-Looie, S., Ghanemi, K., Ebrahimi, B., 2018. Quality evaluation of groundwater resources using geostatistical methods (case study: Central Lorestan plain, Iran). Water Resour. Manag. 32, 3611–3628. https://doi.org/10.1007/s11269-018-2009-2.

Samouelian, A., Cousin, I., Tabbagh, A., Bruand, A., Richard, G., 2005. Electrical resistivity survey in soil science: a review. Soil Tillage Res. 83, 173–193. https://doi.org/10.1016/j.still.2004.10.004.

Shannon, C.E., 1949. Communication in the presence of noise. Proc. Inst. Radio Eng. 37 (1), 10–12.

Shao, S., Guo, X., Gao, C., 2019. Fresh underground light non-aqueous liquid (LNAPL) pollution source zone monitoring in an outdoor experiment using cross-hole electrical resistivity tomography. Environ. Sci. Pollut. Res. 26, 18316–18328. https://doi.org/10.1007/s11356-019-05039-8.

Suthersan, S.S., Horst, J., Schnobrich, M., Welty, N., Mcdonough, J., 2016. Remediation engineering. In: Design Concepts, 2nd edn. CRC Press, Taylor, Francis Group, Boca Raton, pp. 107–135.

Teramoto, E.H., Isler, E., Polese, L., Baessa, M.P.M., Chang, H.K., 2019. LNAPL saturation derived from laser induced fluorescence method. Sci. Total Environ. 683, 762–772. https://doi.org/10.1016/j.scitotenv.2019.05.262.

Totsche, K.U., Kogel-Knabner, I., Haas, B., Scheibke, R., Geisen, S., 2003. Evidence for preferential flow and ageing of NAPL and NAPL borne contaminants in the unsaturated soil zone of a creosote contaminated site: a field study. J. Plant Nutr. Soil Sci. 166, 102–110.

Tran, H., Vu, H.C., Lin, C., Bui, X., Huang, W., Vo, T., Hoang, H., Liu, W., 2018. Remediation of highly fuel oil-contaminated soil by food waste composting and its volatile organic compound (VOC) emission. Bioresour. Technol. Rep. 4, 145–152. https://doi.org/10.1016/j.biteb.2018.10.010.

Trulli, E., Morosini, C., Rada, E.C., Torretta, V., 2016. Remediation in situ of hydrocarbons by combined treatment in a contaminated alluvial soil due to an accidental spill of LNAPL. Sustainability 8, 1086.

Vasudevan, M., Johnston, C.D., Bastow, T.P., Lekmine, G., Rayner, J.L., Nambi, I.M., Suresh Kumar, G., Ravi Krishna, R., Davis, G.B., 2016. Effect of compositional heterogeneity on dissolution of non-ideal LNAPL mixtures. J. Contam. Hydrol. 194, 10–16. https://doi.org/10.1016/j.jconhyd.2016.09.006.

Vozka, P., Modereger, B.A., Park, A.C., Zhang, W., Trice, R.W., Kenttämaa, H.I., Kilaz, G., 2019. Jet fuel density via GC-×-GC-FID. Fuel 235, 1052–1060. https://doi.org/10.1016/j.fuel.2018.08.110.

Wang, W., Huang, L., 2012. 3D geological modeling for mineral resource assessment of the Tongshan Cu deposit, Heilongjiang Province, China. Geosci. Front. 3 (4), 483–491. https://doi.org/10.1016/j.gsf.2011.12.012.

Xia, T., Dong, Y., Mao, D., Meng, J., 2021. Delineation of LNAPL contaminant plumes at a former perfumery plant using electrical resistivity tomography. Hydrogeol. J. 29, 1189–1201. https://doi.org/10.1007/s10040-021-02311-5.

Zeng, J., Li, C., Wang, J., Tang, L., Wu, C., Xue, S., 2022. Pollution simulation and remediation strategy of a zinc smelting site based on multi-source information. J. Hazard. Mater. 433, 128774 https://doi.org/10.1016/j.jhazmat.2022.128774.